Evolution of the galaxy luminosity function at z < 0.3

Evolution of the galaxy luminosity function at $z < 0.3$

Jon Loveday*

Astronomy Centre, University of Sussex, Falmer, Brighton BN1 9QJ

ABSTRACT

We measure the redshift-dependent luminosity function and the comoving radial density of galaxies in the Sloan Digital Sky Survey Data Release 1 (SDSS DR1). Both measurements indicate that the apparent number density of bright galaxies increases by a factor ≈ 3 as redshift increases from $z = 0$ to $z = 0.3$. This result is robust to the assumed cosmology, to the details of the K-correction and to direction on the sky. These observations are most naturally explained by significant evolution in the luminosity and/or number density of galaxies at redshifts $z < 0.3$. Such evolution is also consistent with the steep number-magnitude counts seen in the Automatic Plate Measuring (APM) Galaxy Survey, without the need to invoke a local underdensity in the galaxy distribution or magnitude scale errors.

Key words: galaxies: evolution – galaxies: luminosity function, mass function – galaxies: statistics.

1 INTRODUCTION

Measurements of the galaxy luminosity function (LF) and its evolution provide important constraints on theories of galaxy formation and evolution. It is currently believed that galaxies formed hierarchically from the merger of subclumps, with the peak of star formation rate occurring around redshifts $z \approx 2$–4, e.g. Cole et al. (2000). Since then, galaxies are thought to have evolved mostly passively as their stellar populations age, with occasional activity triggered by interactions with other galaxies.

Significant evolution in the LF has been measured since redshift $z \sim 1$ (e.g. Lilly et al. 1995; Ellis et al. 1996; Wolf et al. 2003), but most existing galaxy samples have been too small to directly constrain evolution at more recent epochs. By combining three different redshift surveys, Eales (1993) was able to demonstrate that the amplitude of the LF increases by a factor ≈ 3 in the redshift range $0 < z < 0.4$. He also found evidence for an increase in the amplitude of the LF to $z \approx 0.15$–0.2, although the strength of this low-redshift evolution was poorly constrained.

The Sloan Digital Sky Survey (SDSS, York et al. 2000), provides an ideal sample with which to measure galaxy evolution at low redshifts. A recent determination of the LF at redshift $z = 0.1$ (Blanton et al. 2003c), allowing for galaxy evolution, showed that the typical r-band galaxy luminosity brightens by ≈ 1.6 mag per unit redshift. Here we further investigate evolution in the r-band LF of SDSS galaxies. We describe the data sample in Section 2 and estimate the LF in four redshift slices in Section 3. The effects of galaxy evolution are investigated in an alternative way in Section 4, where we estimate the radial density of galaxies. Comparisons with observed number-magnitude counts are made in Section 5 and we conclude in Section 6.

*E-mail: J.Loveday@sussex.ac.uk

2 DATA SAMPLE

We use galaxies from the SDSS Data Release 1 (DR1, Abazajian et al. 2003). The SDSS is performing five-band CCD imaging over an area $\sim 10\,000$ deg^2 (Fukugita et al. 1996; Gunn et al. 1998; Hogg et al. 2001; Smith et al. 2002; Pier et al. 2003). A multifibre spectrograph is measuring spectra and redshifts for a subset of sources detected in the imaging data; here we consider only galaxies in the main flux-limited sample (Strauss et al. 2002). A technical summary of the survey is given in York et al. (2000) and a description of SDSS photometric and spectroscopic parameters may be found in Stoughton et al. (2002).

The magnitude limit of the main galaxy survey has been set at an extinction-corrected (Schlegel, Finkbeiner & Davis 1998) r-band Petrosian magnitude $r < 17.77$. This magnitude limit was chosen because test year data demonstrated that it corresponds closely to the desired target density of 90 objects per square degree; see Strauss et al. (2002) for full details of the target selection algorithm. However, a small amount of early data included in DR1 was taken when the magnitude limit was set at $r < 17.6$, and so we adopt this brighter magnitude limit here. We thus select galaxies from the DR1 catalogue with extinction-corrected r-band Petrosian magnitude $r < 17.6$ and with one or more of the TARGET_GALAXY, TARGET_GALAXY_BIG or TARGET_GALAXY_BRIGHT_CORE bits set in the primTarget bit mask; see Stoughton et al. (2002) for a description of these target classifications.

These selection criteria yield a sample of 162 989 target galaxies over 2099 deg^2. Of these target galaxies, 91 921 have had a spectrum observed and 91 611 have a redshift measured with a confidence of 80 per cent or higher. The sampling rate for our sample, defined as the number of galaxies with reliable redshifts divided by the number of target galaxies, is thus $f = 0.562$. This low sampling rate is simply due to the fact that SDSS spectroscopic

observations lag imaging observations; the effective spectroscopic area is 1360 deg^2. The fraction of targets observed spectroscopically is further reduced by limitations on the placement of spectroscopic fibres (Blanton et al. 2003a). The fraction of spectra yielding reliable redshifts is more than 99.6 per cent, with no discernible dependence on apparent magnitude. Whilst we naturally cannot demonstrate that spectroscopic success rate is independent of redshift, the fraction of galaxy spectra without reliable redshifts is only 0.4 per cent, and so spectroscopic incompleteness will have a negligible effect on estimates of galaxy evolution.

Heliocentric velocities are converted to the Galactocentric frame using $v_{\mathrm{Gal}} = v_{\mathrm{Helio}} + 220 \sin(l) \cos(b)$. Unless otherwise stated, we assume a Hubble constant of $H_0 = 100$ km s^{-1} Mpc^{-1} and an $\Omega_{\mathrm{M}} = 0.3$, $\Omega_\Lambda = 0.7$ cosmology in calculating distances, comoving volumes and luminosities.

When estimating intrinsic galaxy luminosities, it is necessary to correct for the fact that a fixed observed passband corresponds to a different range of wavelengths in the rest frames of galaxies at different redshifts, the so-called K-correction. The K-correction depends on the passband used, the redshift of the galaxy and its spectral energy distribution (SED). Here we use KCORRECT v3_1B (Blanton et al. 2003b) in order to estimate and apply these corrections. Briefly, this code estimates an SED for each galaxy by finding the non-negative, linear combination of three template spectra that gives the best fit to the five SDSS magnitudes of that galaxy. Rather than estimating luminosities in the rest-frame of each galaxy, we use KCORRECT to estimate luminosities in a passband blueshifted by $z = 0.1$. Following Blanton et al. (2003b) we denote the r-band in this frame as $^{0.1}r$. The advantage of this choice of restframe is that galaxies at redshift $z = 0.1$ (close to the mean for the SDSS main galaxy sample) have K-corrections independent of galaxy type, and these corrections are on average smaller in amplitude than K-corrections at redshift zero.

3 GALAXY LUMINOSITY FUNCTION

We estimate the LF using the Sandage, Tammann & Yahil (1979, hereafter STY) parametric maximum likelihood method and the stepwise maximum likelihood (SWML) method of Efstathiou, Ellis & Peterson (1988, hereafter EEP). These estimators are unbiased by density inhomogeneities and have well-defined error properties. Both methods assume that $\phi(L)$ has a universal form, i.e. the number density of galaxies is separable into a function of luminosity times a function of position: $n(L, \mathbf{x}) = \phi(L)\, \rho(\mathbf{x})$. Using these estimators, the shape of $\phi(L)$ is determined independently of its normalization.

3.1 Shape

The probability of seeing a galaxy of luminosity L_i at redshift z_i in a flux-limited catalogue is given by

$$p_i \propto \phi(L_i) \left/ \int_{L_{\min}(z_i)}^{L_{\max}(z_i)} \phi(L)\,\mathrm{d}L \right. , \tag{1}$$

where $L_{\min}(z_i)$ and $L_{\max}(z_i)$ are the minimum and maximum luminosities observable at redshift z_i in a flux limited sample. In the STY method, the likelihood $\mathcal{L} = \prod p_i$ (where the product extends over all galaxies in the sample) is maximized with respect to a set of parameters describing the function $\phi(L)$. For example, if we assume that $\phi(L)$ is described by a Schechter (1976) function,

$$\phi(L)\,\mathrm{d}L = \phi^* \left(\frac{L}{L^*}\right)^\alpha \exp\left(-\frac{L}{L^*}\right) \mathrm{d}\left(\frac{L}{L^*}\right), \tag{2}$$

we maximize the likelihood with respect to α and L^*. Errors in the Schechter parameters are estimated by the jackknife method, whereby we subdivide the galaxies into 20 roughly equal subsamples and estimate the Schechter parameters omitting each subsample in turn. The variance in parameter x is then given by

$$\mathrm{Var}(x) = \frac{N-1}{N} \sum_{i=1}^{N} (x - \bar{x})^2, \tag{3}$$

where $N = 20$ is the number of subsamples and $\bar{x}$ is the mean of x.

For the highest redshift subsample considered here, $z > 0.2$, only galaxies more luminous than $M_{0.1_r} \approx -21.5$ make it into the SDSS main galaxy sample. We thus have only a range of about two magnitudes over which to fit the Schechter function. Consequently, the accuracy with which the Schechter parameters can be determined is limited, particularly the value of the faint-end slope α. We therefore also estimate the luminosity function using the SWML method of EEP in which $\phi(L)$ is parameterized as a set of numbers ϕ_k in equally spaced magnitude bins. The likelihood $\mathcal{L}$ is maximized with respect to ϕ_k applying constraints as described in EEP. Also following EEP, errors on the ϕ_k value are estimated from the information matrix.

3.2 Normalization

We use the following estimator of the space density $\bar{n}$ of galaxies:

$$f\bar{n} = \sum_{i=1}^{N_{\mathrm{gal}}} w(z_i) \left/ \int_{z_{\min}}^{z_{\max}} \mathrm{d}V\, S(z) w(z) \right. , \tag{4}$$

where f is the sampling rate, $S(z)$ the galaxy selection function and $w(z)$ a weighting function. The selection function for galaxies with luminosities L_1 to L_2 is

$$S(z) = \int_{\max([L_{\min}(z), L_1])}^{\min(L_{\max}(z), L_2)} \phi(L)\,\mathrm{d}L \left/ \int_{L_1}^{L_2} \phi(L)\,\mathrm{d}L \right. . \tag{5}$$

Note that the integration limits in the numerator depend on the K-correction. In this case, we estimate the K-correction using an SED created from the mean template coefficients of all galaxies in the sample.

We adopt the weighting function

$$w(z) = \frac{1}{[1 + 4\pi f \bar{n} J_3(r_c) S(z)]}, \quad J_3(r_c) = \int_0^{r_c} r^2 \xi(r)\,\mathrm{d}r \tag{6}$$

where $\xi(r)$ is the two-point galaxy correlation function. Provided $J_3(r_c)$ converges on a scale r_c much smaller than the depth of the survey, then the weighting scheme (equation 6) minimizes the variance in the estimate of $\bar{n}$ (Davis & Huchra 1982). Larger values of J_3 weight galaxies at high redshift more highly; we adopt $4\pi J_3 \approx 32\,000\ h^{-3}$ Mpc^3. This value comes from integrating the two-point galaxy correlation function of Zehavi et al. (2002), $\xi(r) = (r/6.14)^{-1.75}$, to $r_c = 50\ h^{-1}$ Mpc; at larger separations the value of J_3 becomes uncertain. However, the results are not too sensitive to the value of J_3, the estimated density decreasing by 7 per cent if J_3 is halved.

When normalizing the non-parametric SWML estimate, the integrals in (5) are replaced by sums over magnitude bins, with appropriate weighting of partial bins in the numerator.

3.3 Results

3.3.1 Full sample

We first estimate the luminosity function for all 90 275 galaxies in the SDSS DR1 with redshifts greater than 0.001 and with absolute
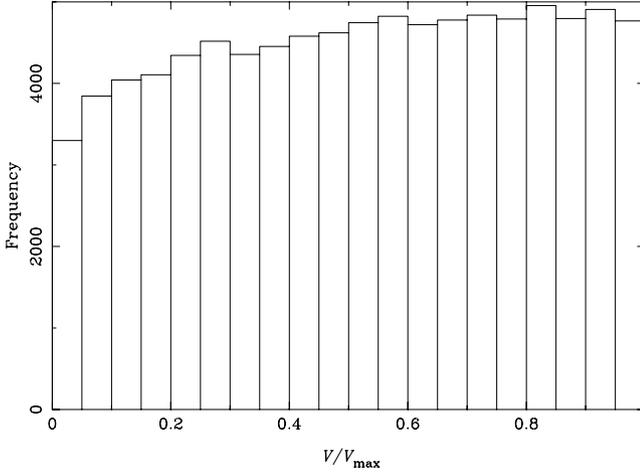
Figure 1. Distribution of the V/V_{max} statistic for all main sample galaxies in SDSS DR1.
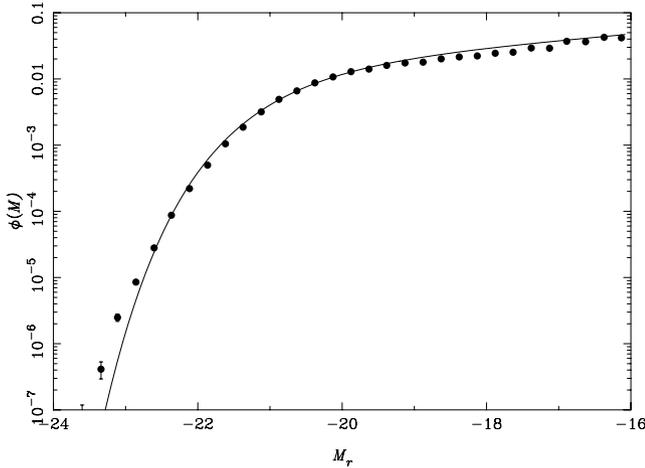

Figure 2. Luminosity function for all main sample galaxies in SDSS DR1. Symbols denote SWML estimates (the error bars are smaller than the symbol size for most of the points) and the curve shows the best-fitting Schechter function. Note that no allowance for evolution has been made in this estimate.

magnitudes in the $^{0.1}r$ band between -24 and -16. The first indication of significant evolution in this sample comes from the skewed distribution of the Schmidt (1968) V/V_{max} statistic (Fig. 1). We find a mean $\langle V/V_{max} \rangle = 0.523$, whereas one would expect $\langle V/V_{max} \rangle = 0.500 \pm 0.001$ for a homogeneous distribution of 90 275 galaxies.

The luminosity function of this full sample is shown in Fig. 2. A Schechter function with parameters $\alpha = -1.23 \pm 0.02$, $M^* = -20.63 \pm 0.02$ and $\phi^* = 0.0194 \pm 0.0010\ h^3$ Mpc^{-3} provides good agreement with the non-parametric SWML estimator except for the bright end, $M_r < -22.5$, where we see in the SWML estimate a higher density of galaxies than predicted by the Schechter function. This bright-end excess can be explained by evolution of the LF: the most luminous (rare) galaxies are likely to be seen at high redshift and, as we shall see below, high-redshift galaxies have an enhanced luminosity or density relative to low-redshift galaxies. The Schechter function fit will be mostly constrained by galaxies at an intermediate redshift ($\bar{z} \approx 0.1$). Additionally, it is possible that some galaxies with extreme luminosities, $M_{0.1_r} \lesssim -23$, may have incorrectly measured fluxes – see below.

Note that any evolution in the luminosity function will render invalid our assumption that the number density of galaxies can be
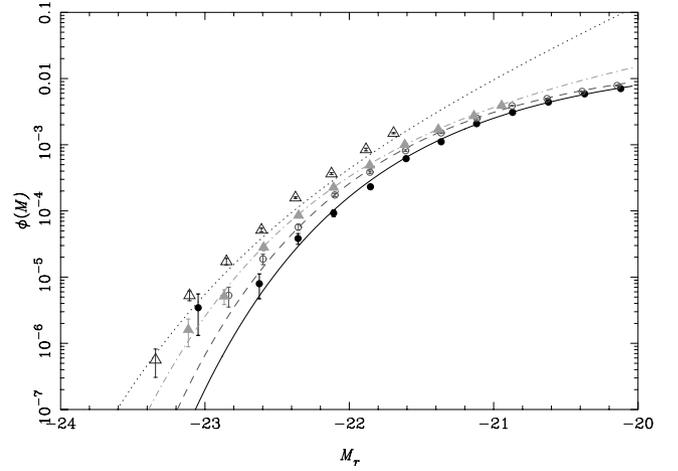
Figure 3. Luminosity function for $z < 0.1$ (filled circles, solid line), $0.1 < z < 0.15$ (open circles, dashed line), $0.15 < z < 0.2$ (filled triangles, dot-dashed line), $0.2 < z < 0.3$ (open triangles, dotted line). This figure can be seen in colour in the on-line version of the journal on *Synergy*.

separated into a function of luminosity times a function of position. In order to obtain an unbiased estimate of the LF, one needs to allow for evolution. Blanton et al. (2003c) have already shown that the *r*-band luminosity function of galaxies in the SDSS can be described by a Schechter function whose characteristic luminosity L^* brightens by ≈ 1.6 mag per unit redshift. Here we investigate the evolution of the galaxy LF in an alternative way, simply by subdividing the sample into slices in redshift.

3.3.2 Redshift slices

Fig. 3 plots the *r*-band luminosity function for galaxies selected in four redshift slices: $0.001 < z < 0.1$, $0.1 < z < 0.15$, $0.15 < z < 0.2$ and $0.2 < z < 0.3$. The points with error bars show the SWML estimates, the lines show the Schechter function fits. Note that one cannot fairly compare the shapes of the Schechter fits from this figure, as the different redshift slices contain galaxies covering a different range of absolute magnitudes. In particular, the faint-end slope of the highest redshift slice is very poorly constrained, because there are no galaxies fainter than $M_{0.1_r} \approx -21.5$ in this subsample. If analysis of the intermediate 0.1–0.15 redshift slice is limited to $M_{0.1_r} < -21.5$, then the estimated faint-end slope changes from $\alpha = -1.17 \pm 0.03$ to -2.18 ± 0.44. The Schechter fits in Fig. 3 are thus included for illustrative purposes only, and we deliberately do not quote the Schechter parameters.

The SWML data point for the lowest redshift slice at $M_{0.1_r} \approx -23$ lies significantly above the Schechter fit. This is almost certainly due to errors in the photometry of the half-dozen or so objects in this bin. Of the 10 apparently most luminous objects in the $z < 0.1$ slice ($M_{0.1_r} \lesssim -22.6$), all have the EDGE or COSMIC_RAY flag set. Low-redshift, luminous galaxies have much larger fluxes and apparent sizes than most galaxies, and hence are more susceptible to their measured fluxes being affected by cosmic ray hits or by lying near the edge of a CCD chip.

Despite the uncertainties in the *shape* of the LF in the redshift slices, there is clear evolution in the *amplitude* of the LF, in the sense of an increasing amplitude (vertical shift) and/or luminosity (horizontal shift) with redshift. The estimated number densities of galaxies in the range $-24 < M_{0.1_r} < -21.5$, obtained by applying (4) to the non-parametric LF for each redshift slice, are given in

Table 1. Number density $\bar{n}$ of galaxies in the range $-24 < M_{0.1_r} < -21.5$, in units of $10^{-4}\ h^3$ Mpc^{-3}. For comparison, $\bar{n}_B$ shows galaxy density inferred from the evolving Schechter LF of Blanton et al. (2003c).

$\bar{z}$	N_{gal}	$\bar{n}$	$\bar{n}_B$
0.078	750	2.48 ± 0.16	2.54 ± 0.07
0.130	2477	3.64 ± 0.15	3.33 ± 0.09
0.178	5559	4.60 ± 0.14	4.21 ± 0.11
0.226	3325	7.36 ± 0.19	5.26 ± 0.14

Table 1. For comparison, we also show the galaxy density inferred from the evolving parametric LF of Blanton et al. (2003c). Their fit gives Schechter parameters $\alpha = -1.05$, $M_0^* = -20.44$ and $\phi^* = 0.0149\ h^3$ Mpc^{-3} at $z_0 = 0.1$ in the $^{0.1}r$ frame, with characteristic magnitude M^* evolving as $M^* = M_0^* - Q(z - z_0)$ with $Q = 1.62$. We ignore the negligibly small number density evolution in their fit and assume that the error in number density is dominated by the ~ 3 per cent uncertainty in ϕ^*. Our density estimates agree within $\sim 2\sigma$ for the three lower redshift slices, but the density estimate for the highest redshift slice is $\sim 9\sigma$ larger than that inferred from the Blanton et al. model. The results presented here, and those of Blanton et al. (2003c), are entirely consistent, as the Blanton et al. parametric model assumed linear evolution of the characteristic magnitude M^* with redshift. Less than 6 per cent of the galaxies in the full ($-24 < M_{0.1_r} < -16$) sample are at $z > 0.2$, and so the Blanton et al. analysis would have been insensitive to rapid evolution at these redshifts.

In the following section, we investigate evolution in the radial density of galaxies in narrower redshift bins. Note that the density estimator we use assumes a non-evolving luminosity function, so any effect found can equally well be ascribed to number or luminosity evolution.

4 RADIAL DENSITY

4.1 Estimator

Just as the maximum-likelihood estimate of the luminosity function $\phi(L)$ is independent of inhomogeneities in the galaxy distribution, one can also estimate the radial density $\rho(z)$ independently of the assumed luminosity function by maximizing the likelihood

$$\mathcal{L} = \prod_i \rho(z_i) \Big/ \int\int_{z_{min}(L_i)}^{z_{max}(L_i)} \rho(z)\,dV\ , \qquad (7)$$

where $z_{min}(L_i)$ and $z_{max}(L_i)$ are the limiting redshifts at which a galaxy of luminosity L_i would still be included in the survey. We fit $\rho(z)$ by an arbitrary step function, using a variant of the SWML estimator (Saunders et al. 1990). As in the maximum-likelihood estimate of $\phi(L)$, overall normalization is lost and so we have applied the constraint

$$\int \rho(z)S(z)w(z)\,dV \Big/ \int\int S(z)w(z)\,dV = 1, \qquad (8)$$

where $S(z)$ is the selection function (5) and $w(z)$ is the weighting function (6). This constraint is also used for the error estimates (cf. EEP).

4.2 Results

Our estimate of $\rho(z)$ is plotted separately for the northern and southern Galactic hemispheres in Fig. 4. We see a gentle increase in $\rho(z)$
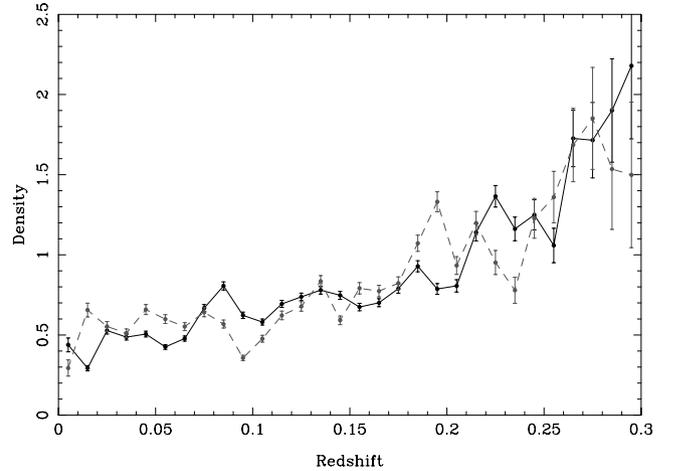

Figure 4. Normalized comoving radial density plotted against redshift for the northern (continuous line) and southern (dashed line) Galactic hemispheres. Note that the radial density is normalized independently for the two hemispheres. This figure can be seen in colour in the on-line version of the journal on *Synergy*.

out to $z \approx 0.2$, with a steeper increase to $z \approx 0.3$. This estimate of radial density is independent of the galaxy luminosity function only insofar as there is no correlation between redshift and luminosity. The observed increase in radial density could thus either reflect an increase in the number density of galaxies at higher redshift (whether due to number density evolution or the existence of a large local 'hole'), and/or an increase in luminosity with redshift. If there is a large local underdensity, it is extremely unlikely that we happen to lie exactly at the centre of it, and so the consistent radial dependence of density in the northern and southern hemispheres provides strong evidence against the local hole hypothesis.

We have also checked the dependence of the estimated radial density on the assumed cosmological model and our method of applying K-corrections. Fig. 5 shows estimated radial density for the full sample (north plus south) for the same assumed cosmology and
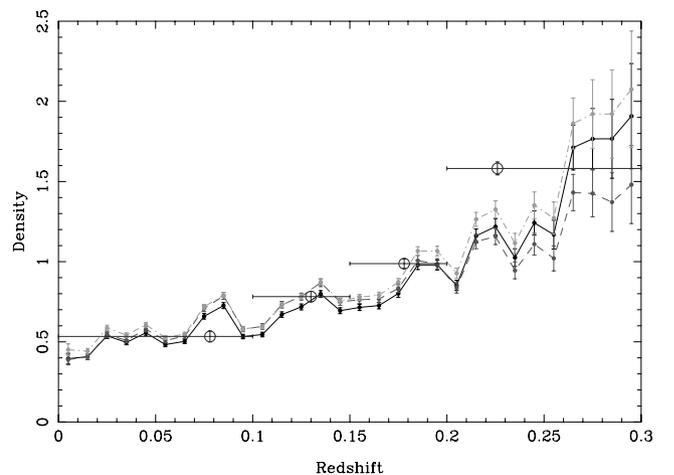

Figure 5. Normalized comoving radial density plotted against redshift for all galaxies assuming the same cosmology and K-correction scheme as Fig. 4 (solid line) and assuming a $\Lambda = 0$ cosmology (dashed line) and K-correcting to the $^{0.0}r$ band (dot–dashed line). The open symbols show normalized densities in the four redshift slices used in the luminosity function analysis (Table 1). This figure can be seen in colour in the on-line version of the journal on *Synergy*.

Table 2. Results of a χ^2 test for uniform density within two redshift ranges (low-z: 0–0.15 and high-z: 0.15–0.3) for the DR1 sample and for clustered and random simulated catalogues. In each case there are 14 degrees of freedom.

Sample	low-z	high-z
DR1	594	1730
Clustered simulation	400	32
Random simulation	14	11

K-correction as Fig. 4, along with the estimate separately assuming a flat, $\Lambda = 0$ cosmology, and K-correcting the r-band galaxy magnitudes to redshift zero instead of redshift $z = 0.1$. The accelerated expansion in the Λ-dominated cosmology gives rise to a larger density at high redshift compared with the $\Lambda = 0$ cosmology. Even though the increase in radial density with redshift is rather less if one assumes a $\Lambda = 0$ cosmology, particularly for $z \gtrsim 0.2$, the increase in density is still significant. The estimated radial density is entirely consistent whether one K-corrects galaxy magnitudes to the $^{0.0}r$ or $^{0.1}r$ bands, suggesting that any errors in the K-correction have a negligible effect on the estimated densities.

We have tested the significance of the radial density evolution over the redshift ranges 0–0.15 and 0.15–0.3. In the lower redshift range, evolution is small but so are the error bars. In the higher redshift range, where evolution is more pronounced, the error bars are much larger. For each redshift range, we calculate the mean radial density and perform a χ^2 test of the null hypothesis that all bins have this mean density. We apply the same test to two non-evolving, simulated catalogues. The first consists of a random distribution of galaxies with comparable galaxy numbers and LF to DR1. The second consists of a Soneira & Peebles (1978) hierarchical simulation with comparable galaxy numbers, LF, clustering and sky coverage to DR1. The resulting χ^2 statistics are given in Table 2; in each case there are 14 degrees of freedom (15 data points minus one free parameter: the mean density).

(i) For the random simulation, the χ^2 values are consistent with the uniform density null hypothesis.

(ii) For the clustered simulation, the χ^2 values are inconsistent with uniform density, particularly in the low-z range. This is to be expected given the presence of large scale structure in the simulated galaxy distribution. The biggest contribution to χ^2 comes from the first three radial bins ($z < 0.03$) where density fluctuations are particularly pronounced since clustering is not smeared out by peculiar velocities in these simulations.

(iii) The DR1 sample yields χ^2 values marginally larger than the clustered simulation in the low-z range, and significantly larger than the clustered simulation in the high-z range. Deviation from a non-evolving $\rho(z)$ is thus clearly very significant in the redshift range 0.15–0.30 but only marginally significant in the redshift range 0–0.15.

4.3 Comparison with LF

The open symbols in Fig. 5 show the densities of luminous galaxies inferred when normalizing the luminosity function in four redshift slices (Table 1), rescaled to have unit mean density. The horizontal bars attached to these symbols denote the redshift range (the symbol is centred on the mean redshift in each bin, rather than at the centre of each bin) and the vertical bars denote the estimated error in density. The agreement between these two completely independent methods of estimating radial density is striking: the apparent increase in estimated radial density with redshift can be explained entirely by evolution of the galaxy luminosity function, with no need for a local underdensity.

5 GALAXY NUMBER COUNTS

In this section we explore the effect of galaxy evolution, as reflected in our estimate of radial density, on counts of galaxies as a function of apparent magnitude. In particular, galaxy number counts in the APM Galaxy Survey (Maddox et al. 1990) are steeper than one would expect unless there is significant evolution of galaxies at low redshift. Can the evolution seen here at $z < 0.3$ explain the steep APM counts?

The predicted number counts per unit magnitude are given by

$$n(m) = \int_0^\infty \phi[L(m, z)]\rho(z)\frac{dV}{dz}\, dz, \tag{9}$$

where $L(m, z)$ is the luminosity of a galaxy at redshift z and with apparent magnitude m, $\rho(z)$ is the radial density and dV is the comoving volume element at redshift z. These predicted counts are plotted in Fig. 6 for the non-evolving LF of Section 3.3.1 with $\rho(z) \equiv 1$ (continuous line) and for the same LF but with $\rho(z)$ as estimated for the full sample in Section 4 (dashed line). We make the conservative assumption when evaluating (9) that density does not evolve further beyond a redshift of 0.3, so that $\rho(z) \equiv 2.0$ for $z > 0.3$.

For comparison, the open circles show number counts measured in the b_J passband from the APM Galaxy Survey (Maddox et al. 1990), where we have made a very rough correction to the r-passband using $r \approx b_J - 1.3$. The evolving model derived from SDSS data is in remarkable agreement with the APM counts considering the different passbands used and areas of sky observed. If the steep APM counts are due to a local underdensity, then a very similar underdensity exists in SDSS galaxy counts which come predominantly from the northern sky.

Observed galaxy number counts from the SDSS Early Data Release (Yasuda et al. 2001) are shown as diamonds (we have summed
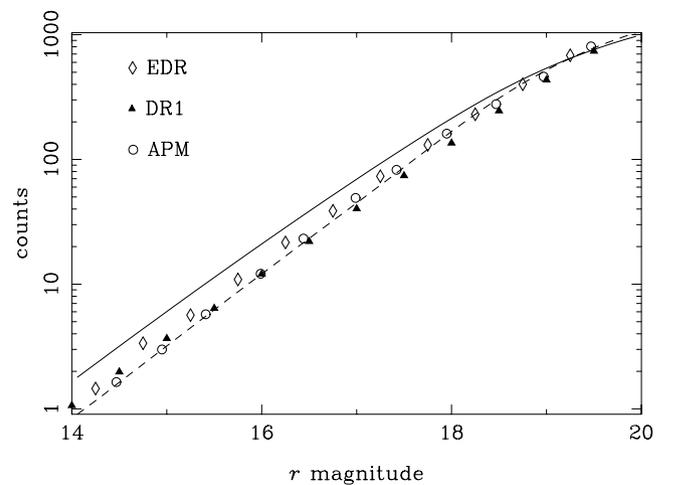

Figure 6. Galaxy counts (per deg^2, per unit magnitude) as a function of r-band magnitude. The continuous line shows predicted counts assuming a non-evolving luminosity function, the dashed line assumes a radial density variation due to evolution as estimated in Section 4. Observed counts are shown by diamonds (EDR), triangles (DR1) and circles (Maddox et al. 1990, APM). For the APM counts, we have applied the very rough correction from b_J to r-band magnitudes $r \approx b_J - 1.3$.

the Yasuda et al. counts in the northern and southern equatorial stripes). These counts are significantly shallower than the APM counts and are consistent in shape with no galaxy evolution. However, these counts come from an area of only 440 deg^2 and so are susceptible to fluctuations from large-scale structure.

We have therefore also estimated galaxy number counts from the 2099 deg^2 of SDSS DR1. Galaxies are selected from the DR1 data base according to the following criteria:

(i) none of the SATURATED, BLENDED, BRIGHT or EDGE bits be set in the *r*-band photoFlags; and

(ii) the object be classified as a galaxy in at least two of the *g*, *r* and *i* bands.

These counts are shown as triangles in Fig. 6. While not quite as steep as the APM counts, they still lie closer to the evolving LF model than to the non-evolving model.

Rapid evolution of the luminosity and/or density of the galaxy population at redshifts $z < 0.3$ thus provides a natural explanation for the observed radial density of SDSS galaxies and steep number counts of APM and DR1 galaxies.

6 CONCLUSIONS

We have presented evidence for significant evolution in the luminosity function of *r*-band selected galaxies in the SDSS DR1 at redshifts $z < 0.3$. This evolution gives rise to a factor $\sim$3 increase in inferred galaxy density between redshifts 0 and 0.3, in agreement with earlier findings from Eales (1993) and Blanton et al. (2003c). Folding this evolution into predictions for galaxy number counts gives a remarkably good match to the slope of number counts observed in the APM Galaxy Survey and in DR1 itself.

The aim of this short paper has simply been to demonstrate that the luminosity function of galaxies has evolved significantly at recent epochs, since $z < 0.3$, and that such evolution is sufficient to explain the steepness of the observed number-magnitude counts of APM galaxies, without the need to invoke a local underdensity or a magnitude scale error.[1]

Note that these results do not preclude the existence of significant density fluctuations in the local Universe on very large scales. Indeed, Frith et al. (2003) have recently used galaxies in the 2 Micron All Sky Survey to indicate the presence of a region in the Southern Galactic hemisphere $\sim$200 h^{-1} Mpc in extent with a mean underdensity $\sim$30 per cent. This underdensity alone, however, is insufficient to explain the steepness of the APM counts. We have shown that evolution of the galaxy LF, possibly in combination with large density fluctuations, can explain the steep counts.

Here we have not attempted to investigate the type of evolution that is occurring: the possibilities include any combination of luminosity evolution, density evolution and change in shape of the galaxy LF. Future work will use SDSS data to study galaxy evolution in detail. We plan to investigate luminosity evolution in different passbands and for different galaxy types, and to perform a detailed investigation of the spectral evolution of galaxies with redshift.

ACKNOWLEDGMENTS

REFERENCES

Abazajian K. et al., 2003, AJ, 126, 2081
Blanton M. R., Lin H., Lupton R. H., Maley F. M., Young N., Zehavi I., Loveday J., 2003a, AJ, 125, 2276
Blanton M. R. et al., 2003b, AJ, 125, 2348
Blanton M. R. et al., 2003c, ApJ, 592, 819
Cole S., Lacey C., Baugh C., Frenk C., 2000, MNRAS, 319, 168
Davis M., Huchra J., 1982, ApJ, 254, 437
Eales S., 1993, ApJ, 404, 51
Efstathiou G., Ellis R. S., Peterson B. A., 1988, MNRAS, 232, 431
Ellis R. S., Colless M., Broadhurst T., Heyl J., Glazebrook K., 1996, MNRAS, 280, 235
Frith W. J., Busswell G. S., Fong R., Metcalfe N., Shanks T., 2003, MNRAS, 345, 1049
Fukugita M., Ichikawa T., Gunn J. E., Doi M., Shimasaku K., Schneider D. P., 1996, AJ, 111, 1748
Gunn J. E. et al., 1998, AJ, 116, 3040
Hogg D. W., Finkbeiner D. P., Schlegel D. J., Gunn J. E., 2001, AJ, 122, 2129
Lilly S. J., Tresse L., Hammer F., Crampton D., Le Fevre O., 1995, ApJ, 455, 108
Loveday J., 2003, MNRAS, 343, 971
Maddox S. J., Sutherland W. J., Efstathiou G., Loveday J., Peterson B. A., 1990, MNRAS, 247, 1P
Pier J. R., Munn J. A., Hindsley R. B., Hennessy G. S., Kent S. M., Lupton R. H., Ivezic Z., 2003, AJ, 125, 1559
Sandage A., Tammann G. A., Yahil A., 1979, ApJ, 232, 352
Saunders W., Rowan-Robinson M., Lawrence A., Efstathiou G., Kaiser N., Ellis R. S., Frenk C. S., 1990, MNRAS, 242, 318
Schechter P. L., 1976, ApJ, 203, 297
Schlegel D. J., Finkbeiner D. P., Davis M., 1998, ApJ, 500, 525
Schmidt M., 1968, ApJ, 151, 393
Smith J. A. et al., 2002, AJ, 123, 2121
Soneira R. M., Peebles P. J. E., 1978, AJ, 83, 845
Stoughton C. et al., 2002, AJ, 123, 485
Strauss M. A. et al., 2002, AJ, 124, 1810
Wolf C., Meisenheimer K., Rix H.-W., Borch A., Dye S., Kleinheinrich M., 2003, A&A, 401, 73
Yasuda N. et al., 2001, AJ, 122, 1104
York D. G. et al., 2000, AJ, 120, 1579
Zehavi I. et al., 2002, ApJ, 571, 172

[1] The possibility of a significant scale error in the APM magnitudes has recently been ruled out using CCD photometry (Loveday 2003).

This paper has been typeset from a TEX/LATEX file prepared by the author.